

Statistical Analysis of the Reaction Progress Variable and Mixture Fraction Gradients in Flames Propagating into Droplet Mist: A Direct Numerical Simulation Analysis

Daniel H. Wacks¹, Nilanjan Chakraborty¹ and Epaminondas Mastorakos²

¹School of Mechanical and Systems Engineering, Newcastle University,
Newcastle-upon-Tyne, Tyne and Wear, UK

²Department of Engineering, University of Cambridge,
Cambridge, UK

1 Introduction

Flame propagation into turbulent droplet-laden mixtures plays a key role in several engineering applications including Internal Combustion engines, aero-gas turbines and the prediction and control of hazards. The experimental evidence [1,2] suggests that flame propagation in turbulent droplet-laden mixtures is a complex physical process depending on the simultaneous interaction of evaporative heat and mass transfer, fluid dynamics and combustion thermo-chemistry. Recently, Direct Numerical Simulations (DNS) have made significant contributions to both the physical understanding and modelling of the combustion of turbulent droplet-laden mixtures [3,4]. Neophytou and Mastorakos [5] recently analysed the effects of volatility, droplet diameter and droplet equivalence ratio on burning velocity in one-dimensional laminar flames where fuel is supplied in the form of mono-disperse droplets. The present analysis extends that of Neophytou and Mastorakos [5] for turbulent flames by carrying out three-dimensional compressible DNS of freely propagating turbulent flame propagation into droplet-laden mixtures. Here the DNS data has been used to analyse the effects of u' , α_d and ϕ_d on the statistical behaviour of the gradients of mixture fraction and reaction progress variable and their interdependence within the flame front when fuel is supplied in the form of droplets on the unburned gas side of the flame and to provide the physical explanations for the observed behaviour.

2 Mathematical Background and Numerical Implementation

A modified single-step Arrhenius-type chemical mechanism, where the activation energy E_{ac} and the heat of combustion are taken to be functions of the gaseous equivalence ratio ϕ_g to account for the correct equivalence ratio dependence of the unstrained laminar burning velocity, is used for the purpose of carrying out an extensive parametric DNS analysis without prohibitive computational cost. The Lewis numbers of all species are taken to be unity and all species in gaseous phase are considered to be perfect gases. Standard values have been used for the ratio of specific heats ($\gamma = C_p^g / C_v^g = 1.4$, where C_v^g (C_p^g) is the gaseous specific heat at constant volume (pressure)) and Prandtl number ($Pr = \mu C_p^g / \lambda = 0.7$). The droplet transport equations are given by [3]:

$$\frac{d\vec{x}_d}{dt} = \vec{u}_d ; \quad \frac{d\vec{u}_d}{dt} = \frac{(\vec{u}(\vec{x}_d, t) - \vec{u}_d)}{\tau_d^p} ; \quad \frac{da_d^2}{dt} = -\frac{a_d^2}{\tau_d^u} ; \quad dT_d/dt = -\frac{(T(\vec{x}_d, t) - T_d - B_d L_v / C_p^g)}{\tau_d^T} \quad (1)$$

where L_v is the latent heat of vaporization, and τ_d^p , τ_d^u and τ_d^T are the relaxation timescales for droplet velocity, diameter and temperature respectively, which are defined as: $\tau_d^p = \rho_d a_d^2 / (18 C_u \mu)$; $\tau_d^u = (\rho_d a_d^2 / 4\mu)(Sc/Sh_c)/\ln(1 + B_d)$ and $\tau_d^T = (\rho_d a_d^2 / 6\mu)(Pr/Nu_c)[B_d/\ln(1 + B_d)](C_p^L/C_p^g)$ where ρ_d is the droplet density, C_p^L is the specific heat for the liquid phase, $C_u = 1 + Re_d^{2/3}/6$ with the droplet Reynolds number Re_d , Sc is the Schmidt number and B_d is the Spalding number, Sh_c is the corrected Sherwood number and Nu_c is the corrected Nusselt number, which are defined as [3]: $Re_d = \rho|\vec{u}(\vec{x}_d, t) - \vec{u}_d|a_d/\mu$; $B_d = [Y_F^s - Y_F(\vec{x}_d, t)]/(1 - Y_F^s)$; and $Sh_c = Nu_c = 2 + 0.555 Re_d Sc / (1.232 + Re_d Sc^{4/3})^{1/2}$ where Y_F^s is the value of fuel mass fraction Y_F at the surface of the droplet. Equation 1 also invokes unity Lewis number assumption. The Clausius–Clapeyron equation for the partial pressure of the fuel vapour at the droplet surface p_F^s is used to evaluate the Spalding number B_d , which leads to following expressions:

$$p_F^s = p_{ref} \exp(L_v/R[(1/T_{ref}^s) - (1/T_d^s)]); \quad Y_F^s = (1 + (W_O/W_F)[p(\vec{x}_d, t)/p_F^s - 1])^{-1} \quad (2)$$

where T_{ref}^s is the boiling point of the fuel at pressure p_{ref} and T_d^s is assumed to be T_d , and W_O and W_F are the molecular weights of oxidiser and fuel respectively. The droplets are coupled to the gaseous phase via additional source terms in the gaseous transport equations as shown below [3,4]:

$$\partial(\rho\varphi)/\partial t + \partial(\rho u_j \varphi)/\partial x_j = \partial[(\rho\nu/\sigma_\varphi)\partial\varphi/\partial x_j]/\partial x_j + \dot{\omega}_\varphi + \dot{S}_\varphi \quad (3)$$

where $\varphi = \{1, u_j, e, Y_F, Y_O\}$ for the conservation equations of mass, momentum, energy and mass fractions respectively, where u_j is the velocity in the j^{th} direction. The $\dot{\omega}_\varphi$ term corresponds to reaction rate and \dot{S}_φ is the appropriate source term due to droplet evaporation, which is linearly interpolated from the droplet's sub-grid position, \vec{x}_d , to the eight surrounding nodes. Other variables are ν , kinematic viscosity, and σ_φ , an appropriate Schmidt number corresponding to φ .

Droplet evaporation leads to mixture inhomogeneities, which can be characterised with the help of mixture fraction defined in terms of fuel and oxidiser mass fractions (i.e. Y_F and Y_O): $\xi = (Y_F - Y_O/s + Y_{O\infty}/s)/(Y_{F\infty} + Y_{O\infty}/s)$, where $Y_{F\infty} = 1.0$ is the fuel mass fraction in the pure fuel stream and $Y_{O\infty} = 0.233$ is the oxidizer mass fraction in air. The hydrocarbon fuel used in this DNS analysis is *n*-heptane, C_7H_{16} , for which $s = 3.52$ and the stoichiometric fuel mass fraction and mixture fraction values are given by $Y_{Fst} = \xi_{st} = 0.0621$. One can furthermore define a reaction progress variable, c , based on a species mass fraction and mixture fraction so that c rises monotonically from 0.0 in unburnt reactants to 1.0 in fully burnt products. In droplet combustion it is advantageous to employ an oxidiser-based reaction progress variable, which takes the following form [4]: $c = [(1 - \xi)Y_{O\infty} - Y_O]/[(1 - \xi)Y_{O\infty} - \max(0, [\xi_{st} - \xi]/\xi_{st})Y_{O\infty}]$. A transport equation of c of the form similar to Eq. 3 may then be derived, in which the reaction rate of c may be defined as:

$$\dot{\omega}_c = [\dot{\omega}_O + \rho N_{\xi\xi}(\partial^2 Y_O/\partial \xi^2) + \rho N_{cc}(\partial^2 Y_O/\partial c^2) + \rho N_{c\xi}(\partial^2 Y_O/\partial c \partial \xi)]/(\partial Y_O/\partial c) \quad (4)$$

where $N_{\zeta_1\zeta_2} = D\nabla\zeta_1 \cdot \nabla\zeta_2$ is the (cross-)scalar dissipation rate, for scalars ζ_1 and ζ_2 (here c or ξ). It is evident from Eq. 4 that the evaluation of (cross-) scalar dissipation rates is essential to accurately model $\dot{\omega}_c$. In the context of Reynolds averaged Navier-Stokes (RANS) simulations, the Favre-averaged (cross-) scalar dissipation rates, $\tilde{\epsilon}_{\zeta_1\zeta_2} = \overline{\rho D\nabla\zeta_1'' \cdot \nabla\zeta_2''}/\bar{\rho}$, must be modelled. Furthermore, in the context of RANS, the gradients of fluctuations are assumed to dominate over mean gradients, giving rise to the approximation $\tilde{\epsilon}_{\zeta_1\zeta_2} \approx \overline{\rho D\nabla\zeta_1 \cdot \nabla\zeta_2}/\bar{\rho} = \tilde{N}_{\zeta_1\zeta_2}$, where $\tilde{N}_{\zeta_1\zeta_2}$ may be expressed in terms of the joint PDF of the scalar gradients as:

$$\tilde{N}_{\zeta_1\zeta_2} = (1/\bar{\rho}) \int_0^\infty \int_0^\infty \rho D \nabla\zeta_1 \cdot \nabla\zeta_2 PDF(|\nabla\zeta_1|, |\nabla\zeta_2|) d|\nabla\zeta_1| d|\nabla\zeta_2|. \quad (5)$$

Equation 5 shows that the statistical behaviours of the scalar gradients, $|\nabla\zeta_1|$ and $|\nabla\zeta_2|$, are of fundamental importance to the successful modelling of $\tilde{\epsilon}_{\zeta_1\zeta_2}$. Thus, the scalars ξ and c and their gradients, $|\nabla\xi|$ and $|\nabla c|$, in statistically planar turbulent flames propagating into a droplet mist have been investigated in the current analysis based on DNS data.

Here a rectangular computational domain of size $30\delta_{th} \times 20\delta_{th} \times 20\delta_{th}$ has been considered for DNS simulations, where $\delta_{th} = (T_{ad} - T_0)/\max(|\nabla\hat{T}|)_L$ (\hat{T} , T_0 and T_{ad} are instantaneous dimensional temperature, unburned gas temperature and adiabatic flame temperature of the stoichiometric mixture respectively) is the unstrained thermal laminar flame thickness of the stoichiometric laminar flame, and the subscript L refers to the values in an unstrained laminar premixed flame for the stoichiometric mixture. The simulation domain for the present analysis is discretised using a Cartesian grid of size $384 \times 256 \times 256$ ensuring about 10 grid points within δ_{th} . This grid is also fine enough to resolve the Kolmogorov length scale η . Partially non-reflecting boundary conditions are used for the mean direction of flame propagation (i.e. x-direction), while the y- and z- directions are considered to be periodic. The droplets are initially distributed uniformly in space throughout the y- and z-directions and in the region $0.0 \leq x/\delta_{th} \leq 10.0$. The reacting flow field is initialised using the steady laminar solution for the required initial values of droplet diameter a_d and droplet equivalence ratio ϕ_d , where a one-dimensional form of the governing equations for the gas and liquid phases are solved in a coupled manner for spray flames, where fuel is supplied in the form of mono-disperse droplets on the unburned gas side of the flame [5]. For the present analysis the unburned gas temperature is taken to be $T_0 = 300\text{K}$, which yields the heat release parameter $\tau = (T_{ad} - T_0)/T_0 = 6.54$, and the fuel is supplied purely in the form of mono-disperse droplets with non-dimensional diameters $a_d/\delta_{th} = 0.06, 0.08, 0.10$ for different values of droplet equivalence ratio: $\phi_d = 1.0, 1.25, 1.5, 1.7$ at a distance $10\delta_{th}$ from the laminar flame. The number of droplets at $t = 0$ varies between $1.16 \leq (\rho_N)^{1/3} \delta_{th} \leq 2.27$, where ρ_N is the droplet number density in the region $0.0 \leq x/\delta_{th} \leq 10.0$. In all cases droplets enter at the left-hand-side of the domain, evaporating as they approach the flame front. Due to the volatility of n-heptane, evaporation starts on entry. The simulations have been carried out under turbulent flow conditions: normalised root-mean-square (rms) turbulent velocities $u'/S_L = 4.0$ and 7.5 and non-dimensional longitudinal integral length scale $L_{11}/\delta_{th} = 2.5$, where S_L is the unstrained laminar burning velocity for the stoichiometric mixture. All simulations are carried out until $t_{final} \approx 2t_{chem} \geq 2t_{turb}$, where $t_{turb} = L_{11}/u'$ and $t_{chem} = \delta_{th}/S_L$ are the initial turbulent eddy turnover time and the chemical time scale, respectively.

3 Results and Discussion

The instantaneous fields of non-dimensional temperature $T = (\hat{T} - T_0)/(T_{ad} - T_0)$, mixture fraction ξ and reaction progress variable c in the central $x - y$ midplane at $t \approx 2t_{chem}$ are shown in Fig. 1 for both $u'/S_L = 4.0$ and 7.5 . However, only the fields arising from the smallest droplets ($a_d/\delta_{th} = 0.06$) and droplet equivalence ratio $\phi_d = 1.0$ are shown. The droplets, depicted as black dots, are those residing in the cells immediately above or below the plane shown in the figure. Full size droplets enter the domain from the left-hand-side and can be seen to shrink in size due to evaporation as they approach the flame front, with some droplets actually penetrating the flame front to complete their evaporation in the burnt gas region. This phenomenon is especially noticeable in cases where the turbulent fluctuations are of greater magnitude and is also evident from the non-dimensional temperature field (left-hand pane) which shows greater inhomogeneities on the burnt gas side as the turbulent fluctuations increase. This is due to the evaporation of droplets which absorbs latent heat from the surrounding gas and thereby reduces the temperature. A comparison between the mixture fraction and reaction progress variable fields (middle and right-hand panes, respectively) reveals that the unburned gas side of the flame remains predominantly fuel-lean. This is true for all cases considered here. On the burnt gas side, however, the same comparison shows the existence of locally fuel-rich regions. These are the result of droplet penetration through the flame front; a phenomenon which is enhanced by the turbulent nature of the flow. The droplets continue to evaporate on the burnt

gas side, but the evaporated gas is not consumed unless it diffuses back towards the flame front, leading to the development of the aforementioned fuel-rich regions.

The PDFs of the mixture fraction ξ are shown in Fig. 2 for all droplet sizes ($a_d/\delta_{th} = 0.06, 0.08, 0.10$) and both turbulent intensities ($u'/S_L = 4.0, 7.5$) for one value of droplet equivalence ratio ($\phi_d = 1.0$) at several locations across the flame brush ($\bar{c} = 0.1, 0.5, 0.9$). Figure 2 shows that the nature of the PDFs varies significantly with position in the flame and that in all cases the most likely mixture shifts from fuel-lean on the unburnt gas side ($\bar{c} = 0.1$) to stoichiometric ($\xi_{st} = 0.0621$)/ fuel-rich on the burnt gas side ($\bar{c} = 0.9$). In the mid-region ($\bar{c} = 0.5$), smaller droplet cases exhibit a tendency to show stoichiometric/fuel-rich mixtures due to higher rate of evaporation, whereas larger droplet cases remain fuel-lean. Furthermore, the PDFs of ξ for cases with lower turbulence intensity ($u'/S_L = 4.0$), although following closely the PDFs of the cases with higher turbulence intensity ($u'/S_L = 7.5$) both in shape and magnitude, show consistently a higher probability of a more fuel-lean mixture at all locations in the flame. In order to model the PDF of ξ , a presumed β -function PDF approach is often considered. The β -function PDF of a scalar ζ is defined as $f(\zeta; a, b) = 1/B(a, b) \zeta^{a-1} (1 - \zeta)^{b-1}$, where $B(a, b) = \int_0^1 \zeta^{a-1} (1 - \zeta)^{b-1} d\zeta$ is a normalization factor with $a = \bar{\xi} [\bar{\xi} (1 - \bar{\xi}) / \bar{\xi}^2 - 1]$ and $b = a / \bar{\xi} - a$, where $\bar{\xi} = \overline{\rho \xi} / \bar{\rho}$ is the Favre averaged mixture fraction. Figure 2 shows that the β -function reasonably captures the general shape and magnitude of the PDFs obtained from DNS data.

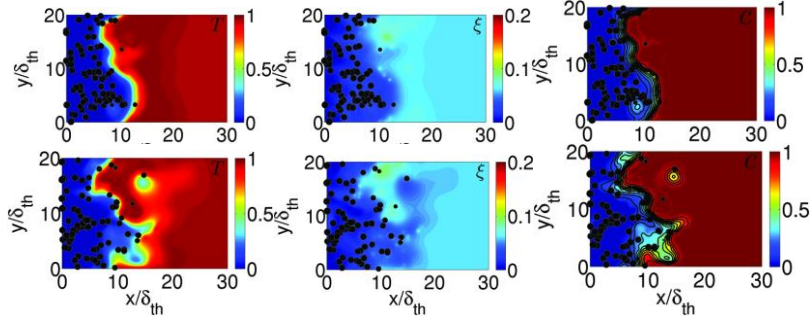


Figure 1. Instantaneous mid- z -plane fields for $a_d/\delta_{th} = 0.06$ and $\phi_d = 1.0$ (left to right) T , ξ and c (black lines show (left to right) contours $c = 0.1 - 0.9$ in steps of 0.1) for $u'/S_L = 4.0$ (top) and 7.5 (bottom). Droplet size is not to scale.

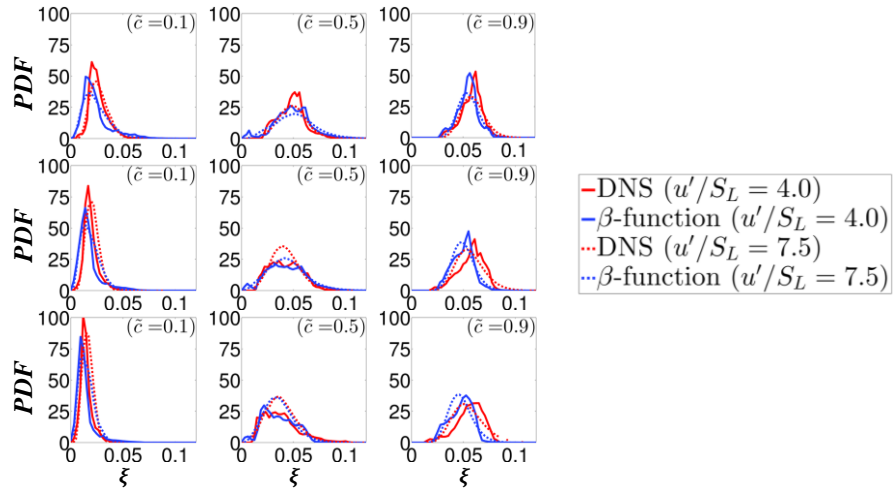


Figure 2. Comparison of PDFs of mixture fraction ξ at (left to right) $\bar{c} = 0.1, 0.5$ and 0.9 for droplet sizes (top to bottom) $a_d/\delta_{th} = 0.06, 0.08, 0.10$ at $\phi_d = 1.0$ with $u'/S_L = 4.0$ and 7.5 showing DNS data and β -function.

Figure 3 shows the PDFs of c across the flame brush for the case $a_d/\delta_{th} = 0.06$ with $\phi_d = 1.0$. All locations in the flame shown here exhibit an almost monomodal distribution: on $\bar{c} = 0.1$ it is most likely to achieve a value $c = 0$, whereas both $\bar{c} = 0.5$ and $\bar{c} = 0.9$ show a strong likelihood of

achieving a value $c = 1$, which increases with increasing \tilde{c} . The β -function PDF parameterised in terms of \tilde{c} and c'^2 is found to reasonably capture the general shape and magnitude of the progress variable PDFs obtained from DNS data.

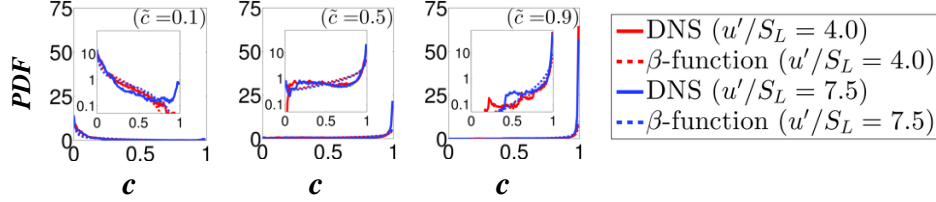


Figure 3. PDFs of c at (left to right) $\tilde{c} = 0.1, 0.5, 0.9$ for droplet size $a_d/\delta_{th} = 0.06$ at $\phi_d = 1.0$ with $u'/S_L = 4.0$ (red) and $u'/S_L = 7.5$ (blue). Insets show log-linear plots.

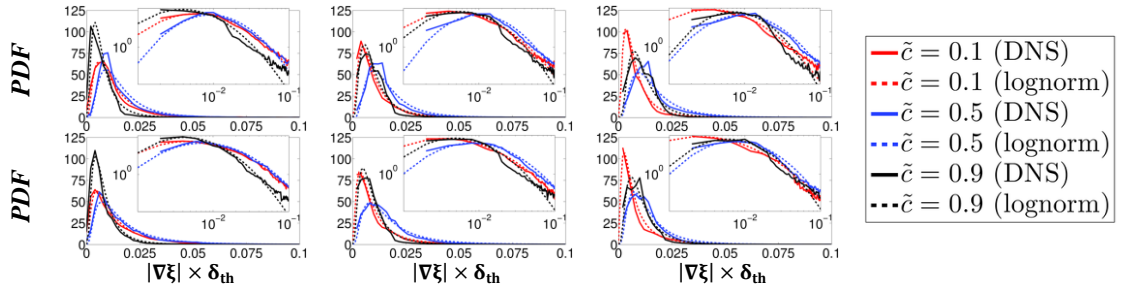


Figure 4. Comparison of PDFs of $|\nabla\xi|$ across the flame brush between DNS data and lognormal distribution for droplet sizes (left to right) $a_d/\delta_{th} = 0.06, 0.08, 0.10$ at $\phi_d = 1.0$ where (top) $u'/S_L = 4.0$ and (bottom) $u'/S_L = 7.5$. Insets show log-log plots.

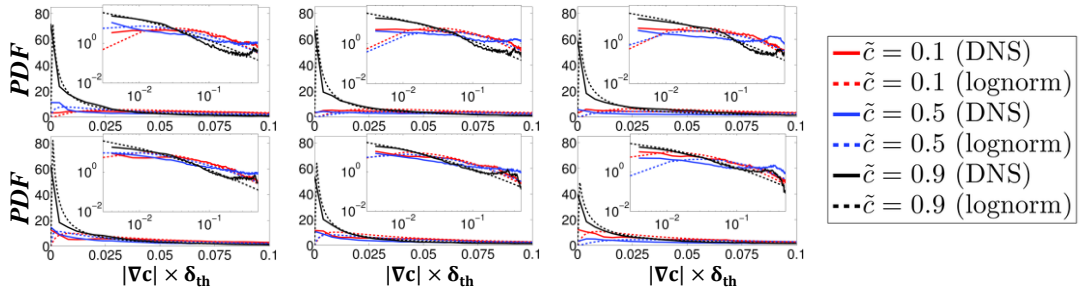


Figure 5. Comparison of PDFs of $|\nabla c|$ across the flame brush between DNS data and lognormal distribution for droplet sizes (left to right) $a_d/\delta_{th} = 0.06, 0.08, 0.10$ at $\phi_d = 1.0$ where (top) $u'/S_L = 4.0$ and (bottom) $u'/S_L = 7.5$. Insets show log-log plots.

Figures 4 and 5 show the PDFs of $|\nabla\xi|$ and $|\nabla c|$, respectively. Often a presumed log-normal distribution is used to model these PDFs. The log-normal distribution of a scalar, ζ , is given by $f(\zeta, \mu', \sigma') = (1/\zeta\sigma'\sqrt{2\pi}) \exp(-(\ln\zeta - \mu')^2/2\sigma'^2)$, where μ' and σ' are mean and standard deviation of the natural logarithm of ζ . Figures 4 and 5 show that both qualitatively and quantitatively the log-normal distribution succeeds in capturing the PDFs of the DNS data. The only exception takes place at high values of $|\nabla\xi|$ and $|\nabla c|$ where there is insufficient data in the DNS dataset to accurately predict the value of the PDF and the regions with high probability of finding $|\nabla c| \approx 0$ which log-normal distribution fails to predict. The discrepancy between the log-normal distribution and the tail of the scalar gradient PDFs is consistent with several previous findings in the context of passive scalar mixing, non-premixed and partially-premixed combustion (see Ref. [7] for further discussion). Finally, Fig. 6 shows joint PDFs of $|\nabla\xi|$ and $|\nabla c|$, $PDF(|\nabla c|, |\nabla\xi|)$, across the flame brush for one case ($a_d/\delta_{th} = 0.06$, $\phi_d = 1.0$, $u'/S_L = 7.5$). Other cases display the same qualitative behaviour. No clear correlation is apparent between $|\nabla\xi|$ and $|\nabla c|$, which is consistent with a previous analysis [7]. Although the absence of correlation does not necessarily mean statistical independence, the similarity between $PDF(|\nabla c|, |\nabla\xi|)$ and $PDF(|\nabla c|) \cdot PDF(|\nabla\xi|)$ suggests that statistical independence of $|\nabla\xi|$

and $|\nabla c|$ might be a valid assumption for these flames, and that the joint PDF can be modelled as $PDF(|\nabla c|) \cdot PDF(|\nabla \xi|)$. This is supported by Fig. 7, in which the joint PDF extracted from the DNS data is modelled by a lognormal bivariate distribution (see Ref.[7] for equations) of $|\nabla c|$ and $|\nabla \xi|$, both under the assumption that the data is correlated (i.e. assuming that the joint PDF is lognormally distributed) and that it is uncorrelated (i.e. assuming only that the individual PDFs are lognormally distributed). A comparison between Figs. 6 and 7 reveals greater agreement between the joint PDF and the lognormal bivariate distribution without correlation.

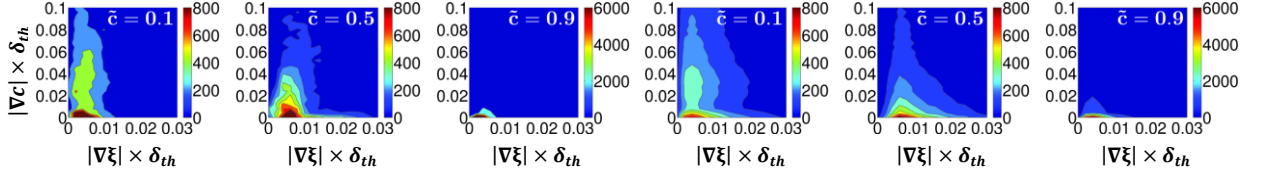


Figure 6. Joint PDF($|\nabla c|$, $|\nabla \xi|$) (columns 1-3) and $PDF(|\nabla c|) \cdot PDF(|\nabla \xi|)$ (columns 4-6) at $\bar{c} = 0.1, 0.5$ and 0.9 for droplets of size $a_d/\delta_{th} = 0.06$ and $\phi_d = 1.0$ where $u'/S_L = 7.5$.

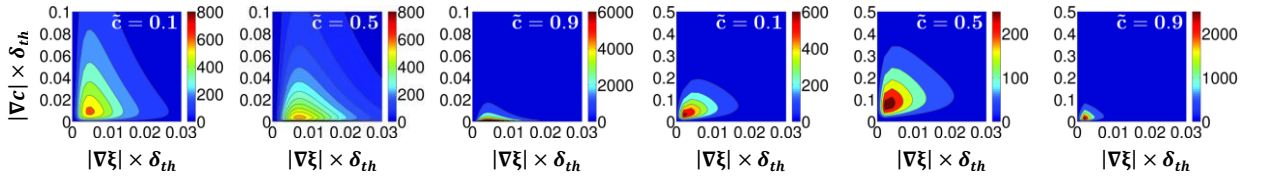


Figure 7. Lognormal bivariate distribution of $|\nabla c|$ and $|\nabla \xi|$ assuming no correlation (columns 1-3) and assuming correlation (columns 4-6) for the case in Fig. 6.

4 Conclusions

The effects of droplet size, droplet equivalence ratio and turbulence intensity on the statistical properties of the scalars ξ and c and their gradients, $|\nabla \xi|$ and $|\nabla c|$, in statistically planar flames propagating into a liquid fuel droplet mist under decaying turbulence have been analysed. It has been shown that a β -function distribution accurately predicts the shape and magnitude of the PDFs of ξ and c , and a log-normal distribution predicts the qualitative behaviour of the PDFs of $|\nabla \xi|$ and $|\nabla c|$, but there exist discrepancies between the log-normal distribution and DNS data at the tails of the PDFs. It has furthermore been found that the correlation between $|\nabla \xi|$ and $|\nabla c|$ remains small and that $PDF(|\nabla c|) \cdot PDF(|\nabla \xi|)$ reasonably approximates the joint PDF, $PDF(|\nabla c|, |\nabla \xi|)$.

References

- [1] Burgoyne JH, Cohen L. (1954). The effect of drop size on flame propagation in liquid aerosols. Proc. Roy. Soc. Lond. A. 225:375.
- [2] Lawes M, Saat A. (2011). Burning rates of turbulent iso-octane aerosol mixtures in spherical flame explosions. Proc. Combust. Inst. 33:20-47.
- [3] Reveillon J, Vervisch L. (2000). Spray vaporization in non-premixed turbulent combustion modelling: a single droplet model. Combust. Flame. 121:75.
- [4] Neophytou A, Mastorakos E, Cant RS. (2010). DNS of spark ignition and edge flame propagation in turbulent droplet-laden mixing layers. Combust. Flame. 157:1071.
- [5] Neophytou A, Mastorakos E. Simulations of laminar flame propagation in droplet mists. Combust. Flame. 156:1627.
- [6] Tarrazo E, Sanchez A, Linan A, Williams FA. (2006). A simple one-step chemistry model for partially premixed hydrocarbon combustion. Combust. Flame. 147:32.
- [7] Malkeson SP, Ruan S, Chakraborty N, Swaminathan N. (2013). Statistics of reaction progress variable and mixture fraction gradients from DNS of turbulent partially premixed flames. Combust. Sci. Tech. 185:1329.